J Mater Sci (2011) 46:2982–2990
DOI 10.1007/s10853-010-5175-z

Effect of Mn and P on precipitation behavior and solute distribution in ultra-low carbon bake hardening steels

Hua Wang · Naqiong Zhu · Wen Shi · Lin Li · Rendong Liu

Received: 26 August 2010 / Accepted: 8 December 2010 / Published online: 29 December 2010

Abstract The effect of Mn and P on types of precipitates as well as solute distributions in ultra-low carbon bake hardening (ULC-BH) steels was originally investigated in this paper. Three samples of hot-rolled ULC-BH steels (Ti–V, Ti–V–Mn, and Ti–V–P) were prepared. The types of precipitates in the three samples were characterized with scanning electron microscopy (SEM) and transmission electron microscopy (TEM), and further calculated by *Thermo-Calc*. The different types of nanometer sized vanadium carbides are clearly characterized by SEM and TEM, and results of calculation and experiments are generally in agreement. Besides, the solute distributions in Ti–V–Mn and Ti–V–P steels were detected by three-dimensional atom probe (3DAP). It is found that no Ti, N, or S elements are present in both of the two steels, and the distribution patterns of the solute elements in the two steels are completely determined. Results show that SEM, TEM combining with 3DAP can well detect the existence of elements added into the bake hardening steels, and are very useful techniques for the base of the further investigation of mechanical properties and bake hardening phenomenon in bake hardening steels.

H. Wang · N. Zhu · W. Shi · L. Li
College of Materials Science and Engineering, Shanghai University, Shanghai 200072, China

R. Liu
Ansteel Group Co, Anshan 114021, China

H. Wang (✉)
Room 403, Metal Building, No. 149, Shanghai University, Yanchang Road, Shanghai 200072, China
e-mail: tianyacaiyun@hotmail.com

Introduction

As an excellent member of automotive body panel materials, various types of bake-hardenable steels have been developed since 1981 [1]. It is well known that the first generation of ultra-low carbon bake hardening (ULC-BH) steel was alloyed with Ti and/or Nb [2]. Recently, research focused on vanadium bearing ULC-BH steel has aroused great interest [2–7] because of the lower solution temperature of vanadium than that of niobium carbide, which endows it the advantage of corresponding lower energy consumption during the continuous annealing process. Meanwhile, research on the structures and chemical compositions of precipitates [8, 9], as well as the distribution of solute elements are very important for V-contained ULC-BH steels, as they directly affect the concentrations of added micro alloy elements and the behavior of BH phenomenon.

A variety of studies have been carried out on the precipitation behavior and the properties of resulting precipitates in ULC-BH steels [1–3, 5]. Ooi and Fourlaris [3] have studied the precipitation of VC particles, and the results showed that VC particles were formed during the coiling process and thereafter were dissolved in the following continuous annealing cycles. However, few researches on the influence of Mn and P on the precipitation behavior of vanadium carbides have been reported.

Moreover, three-dimensional atom probe (3DAP) is the only instrument that currently can identify the identities of individual atoms in a material and measure their spatial coordinates with resolution close to 0.3 nm [10]. Several studies about using 3DAP to perform microanalysis of materials are reported [11–20]. Ohkubo and co-workers [16] detected pairs of plate-like precipitates in an age-hardened Mg–Ca–Zn alloy by 3DAP, and determined the

lattice plane of these precipitates laid on as well as their chemical composition and concentration. Pereloma et al. [19] used 3DAP to analyze the solute distribution in TRIP steels, and obtained the partitioning of elements between different phases and microconstituents. Although lots of studies on the concentration of solute carbon element by the calculation of internal friction have been previously reported [5, 21–23], few researches about using micro-analysis technique to determine the distribution of solute C in ULC-BH steels are conducted.

Hot-rolled ULC-BH steels were selected as object of study because most precipitates formed during hot rolling process tend to be steady except for the decomposition of vanadium carbides during annealing processes [2], which makes it possible to further study the composition of resulting precipitates and distribution patterns of solute elements after hot-rolling. The morphologies and chemical compositions of the precipitates were analyzed with scanning electron microscopy (SEM) and transmission electron microscopy (TEM). Then, *Thermo-Calc*, a powerful software package for the calculation of phase equilibriums in multi-component systems, was employed to calculate the mole fractions and compositions of the precipitates in the three hot-rolled ULC-BH steels, and the result is only an assistant explanation for the SEM and TEM result since the calculation is in equilibrium state which is different from the real state. Furthermore, the distribution patterns of solute elements in ULC-BH steels were determined by 3DAP.

Experimental procedure

Samples of the three ULC-BH steels (Ti–V, Ti–V–Mn, and Ti–V–P) were prepared with different contents of P and Mn, and the contents of vanadium and other elements were kept without significant change. Sample of Ti–V steel was prepared with little addition of P and Mn, sample of Ti–V–Mn steel with 1.44 wt% Mn but quite small amount of P, and sample of the Ti–V–P steel with 0.054 wt% P and quite little addition of Mn. Detailed chemical composition of each sample is tabulated in Table 1.

For the preparation of each sample of ULC-BH steel, steel was melted in a vacuum induction furnace and poured into a spindle, which was then forged into 25-mm thick flats and hot-rolled into 4.5-mm thick strips with a finishing temperature of 930 °C followed by air-cooling.

Scanning electron microscopy (SEM; S-570) was performed to observe micron-sized particles, and specimens for this test were etched with 3% nital. Meanwhile, energy dispersive X-ray spectroscopy (EDS) was employed to detect chemical compositions of precipitates, and TEM JEM-2010 F was first used to observe the morphology of nanometer-sized particles; JEM-2010 was then used as a substitute to observe particles because of the limiting experimental conditions. *Thermo-Calc* software was employed to calculate mole fractions of the precipitates as functions of precipitation temperatures in the three steels in equilibrium state. Moreover, 3DAP was used to determine the distribution of solute elements in the three ULC-BH steels. Bars with dimension of 0.5 mm × 0.5 mm × 50 mm were cut from the hot-rolled steel samples and then electropolished to make sharp needle-like specimens for atom probe analysis.

Experimental results and discussions

SEM results and discussions

Results obtained from SEM and EDS analysis indicate that the most common precipitates in the three ULC-BH steels are titanium nitride, concluded from Fig. 1a, b, and the compound shown in Fig. 1c, d might be manganese sulfide, titanium sulfide, and/or a little vanadium carbides and Al_2O_3. Besides, the Al added in the three steels presents mainly as Al_2O_3 which is concluded from Fig. 1e, f; so the effect of Al on other precipitation behaviors in the three steels is very little. The sizes of most of the particles in SEM are about 1 μm.

In Ti–V steel, there are few micron-sized particles, which lie mostly in the matrix rather than on the grain boundaries.

However, in Ti–V–Mn steel, there are more micron-sized particles than those in Ti–V steel, and similar to the particles in Ti–V steel, most of the particles in Ti–V–Mn steel also exist as intragranular precipitates. Apart from the above two common precipitates in the three ULC-BH steels, there are still other precipitates present in Ti–V–Mn steel, which are mostly isolated manganese sulfide particles

Table 1 Chemical composition of the experimental steels (wt%)

	C	N	Mn	S	Si	P	Al	V	Ti
Ti–V	0.0079	0.0027	0.06	0.011	0.062	0.009	0.086	0.090	0.014
Ti–V–Mn	0.0123	0.0057	1.44	0.011	0.064	0.009	0.061	0.090	0.013
Ti–V–P	0.0137	0.0033	0.07	0.008	0.072	0.054	0.12	0.090	0.021

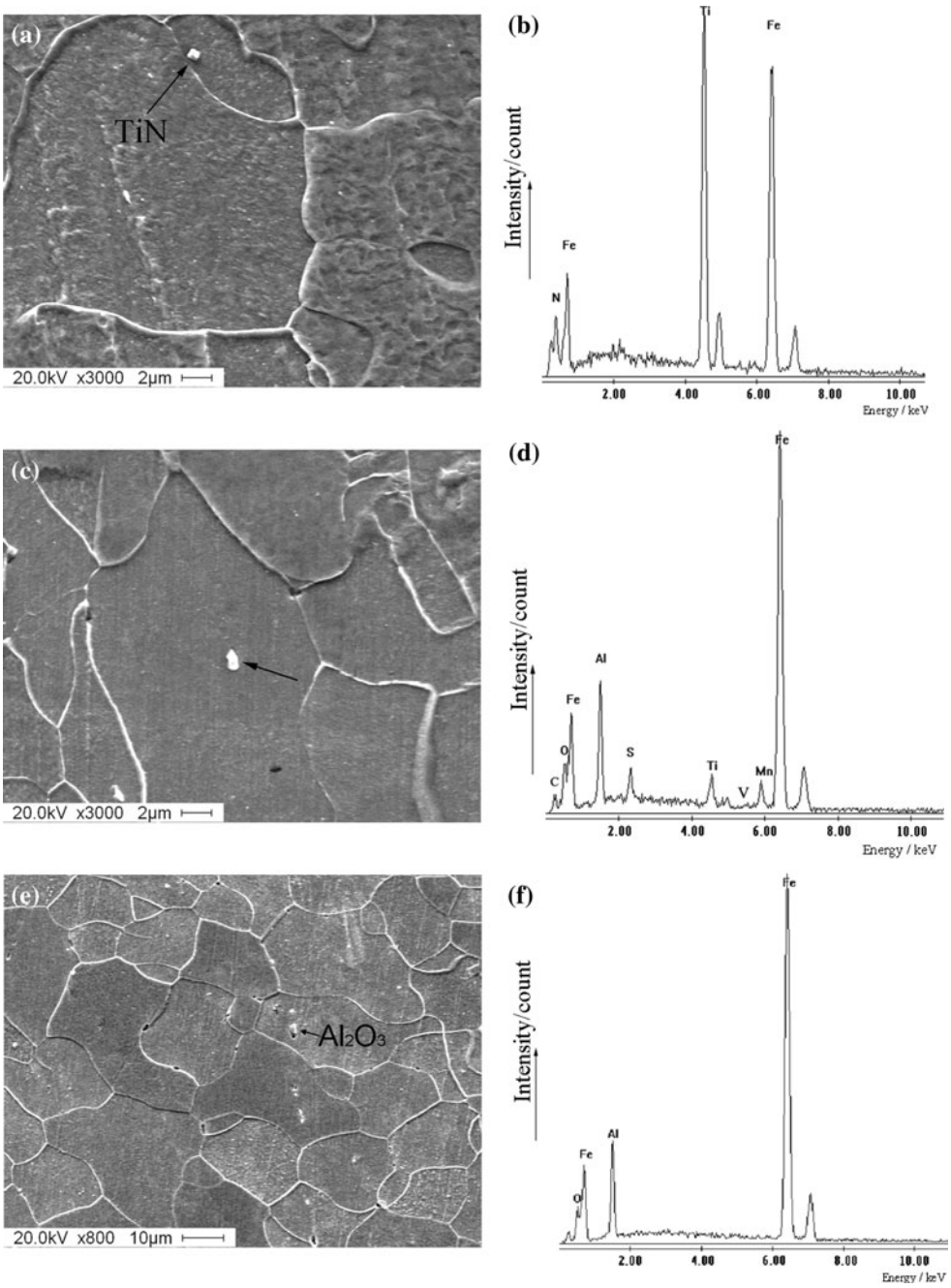

Fig. 1 SEM micrographs showing precipitates and corresponding EDS microanalysis of **a**, **b** TiN and **c**, **d** compound of TiS and MnS and **e**, **f** Al_2O_3 in the three hot-rolled ULC-BH steels

with cone shape (see Fig. 2a, b) and a little titanium carbides (see Fig. 2c, d). Furthermore, a complicated compound which might be $(Mn_xFe_{1-x})_3C$ and oxide are found in Ti–V–Mn steel (see Fig. 2e, f), and the composition (at.%) of it is: C (27.3 at.%), O (7 at.%), Mn (1.2 at.%), and Fe (64.5 at.%). From the composition, it can be concluded that some C will be consumed because of the complicated compound formation. Since this consumption of C will decrease the C concentration and further affect the BH value of BH steel, attention should be paid to the addition of Mn from two aspects, that is, the influence on the total strength of resulted sample and the BH value of the BH steel. The results of Figs. 1 and 2 meet well with the forming tendency order that Ti combine S to precipitate after N is fixed by it [24].

In Ti–V–P steel, there are a similar number of particles comparing with that in Ti–V–Mn steel. However, a considerable number of the particles lie near grain boundaries in Ti–V–P steel, which is very different from those in Ti–V and Ti–V–Mn steels. Apart from the above two common precipitates in the three ULC-BH steels, there are more vanadium carbides precipitate over the compound of

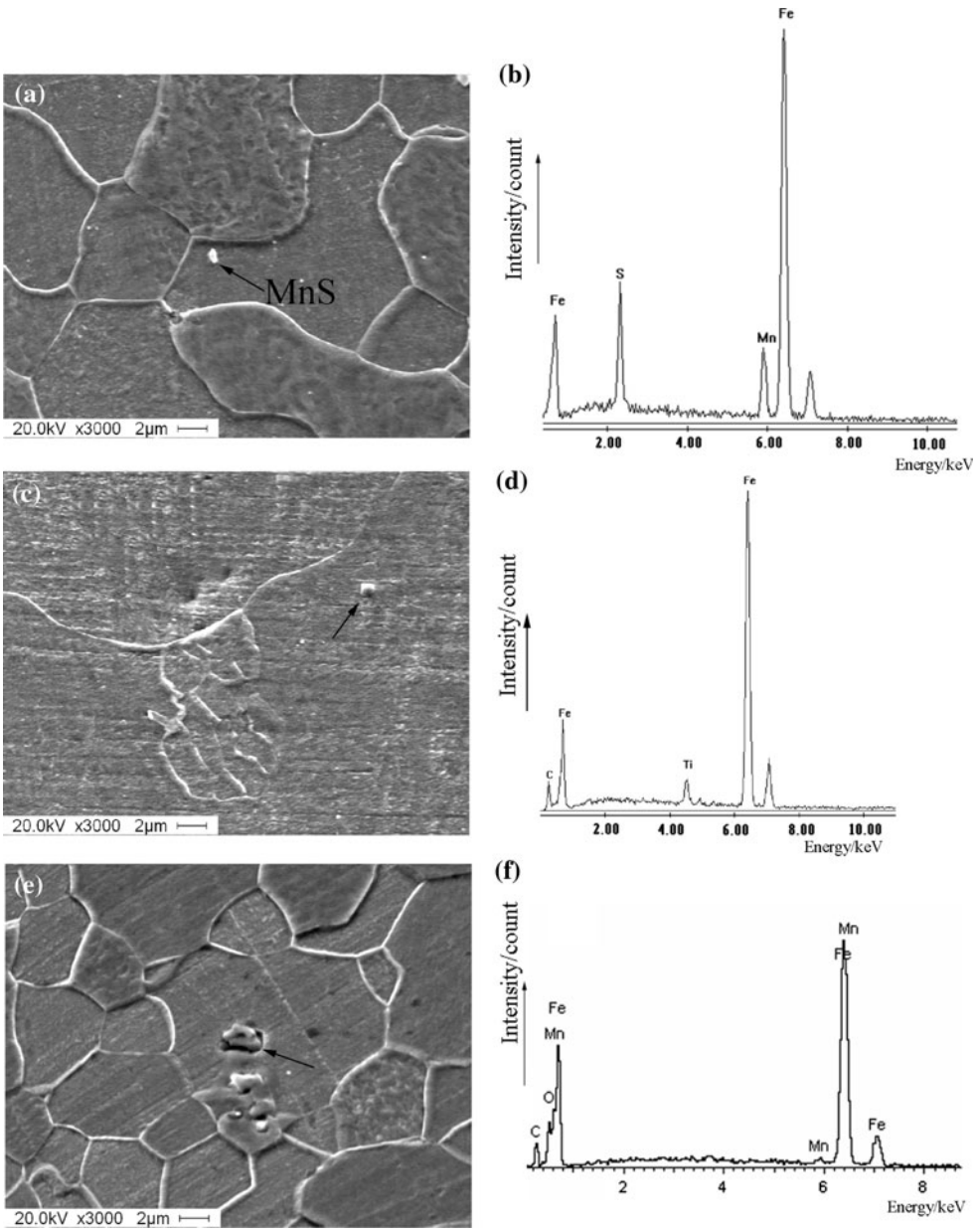

Fig. 2 SEM micrographs and corresponding EDS microanalysis showing precipitates of **a**, **b** MnS, **c**, **d** TiC, and **e**, **f** complicated compound in Ti–V–Mn steel

manganese sulfide and titanium sulfide, and the precipitation order is determined according to the calculation result which will be presented in "Thermodynamic modeling" section. However, no particles containing P element are found in the SEM result even though the bulk concentration of P is high up to 0.054 wt%.

TEM results and discussions

Ti–V steel

The TEM results of Ti–V steel (Fig. 3) reveal that there are a few nanometer-sized particles in the matrix and most of them are titanium nitrides. The Ti–N compound form is Ti_2N rather than TiN, as the mole fraction of Ti added into the matrix is higher than that of N. According to the TEM micrographs, the shape of Ti_2N is cubic, a typical shape of titanium nitrides.

Ti–V–Mn steel

In Ti–V–Mn steel, there are some particles of vanadium carbides with size of only several nanometers as shown in Fig. 4a, b, the theory explanation for which has been mentioned in [25]. The compound forms of them are V_2C and V_6C_5. Moreover, particles of compounds of MnS and TiS are present in this steel (see Fig. 4c, d).

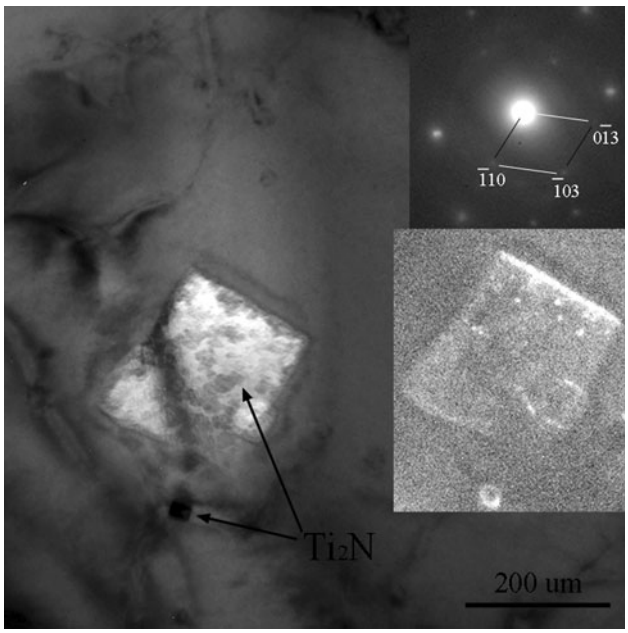

Fig. 3 Ti_2N in Ti–V steel, as depicted by bright field and dark field TEM micrographs

Ti–V–P steel

In Ti–V–P steel, the nanometer-sized particles are mostly manganese sulfides and titanium sulfides. The isolated titanium sulfides, compound of manganese sulfides, and titanium sulfides (or $Ti_4C_2S_2$) are spherical in shape as shown in Fig. 5a, b–e, and f, respectively, and this shape is different from that of the isolated MnS particles in Ti–V–Mn steel (Fig. 2a). The compound of MnS and TiS observed by TEM is also present in the SEM result, and the two results meet well. Moreover, according to the results of SEM and TEM shown in Figs. 1 and 5, most of the vanadium carbides precipitate over the compounds of manganese sulfide and titanium sulfide rather than exist alone.

However, it is clearly shown that there is no FeTiP precipitate in Ti–V–P hot-rolled steel, which is consistent with SEM results, and this phenomenon is also previously reported by Ghosh et al. [26]. (The presence of P in Ti–V–P steel determined by 3DAP will be discussed in the following section.)

Thermodynamic modeling

Thermo-Calc software with database TCFE6 [27] is employed to simulate the precipitation behavior of each experimental steel [28, 29], assuming that the steels are under equilibrium condition.

Calculation results of the mole fractions of precipitates expected to be formed at various annealing temperatures in Ti–V, Ti–V–Mn and Ti–V–P steels are shown in Figs. 6, 7, and 8, respectively.

As a typical example, computing process for Ti–V steel can be described as follows. Mole fractions of MnS and $Ti_4C_2S_2$ are calculated directly in a temperature range from 500 K to 1850 K, since their compositions are clearly defined in TCFE6 database. However, without the discrimination of temperature ranges, the calculation results of Ti and V carbonitrides are denoted as the same symbol,

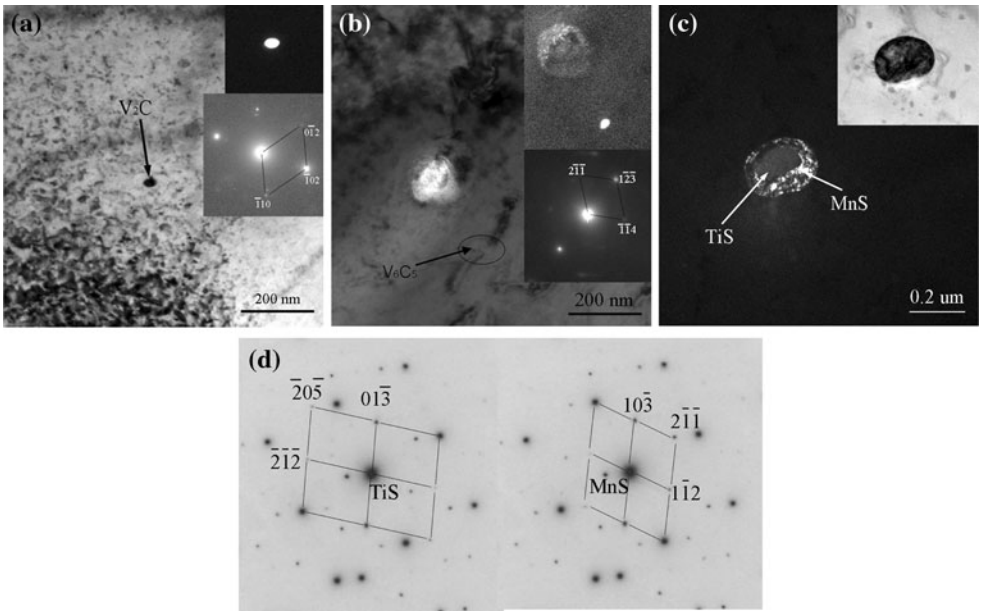

Fig. 4 Precipitates, as depicted by bright field and dark field TEM micrographs, electron diffraction pattern, EDS spectrum of **a** V_2C, **b** V_6C_5 and **c**, **d** compound of MnS and TiS in Ti–V–Mn steel

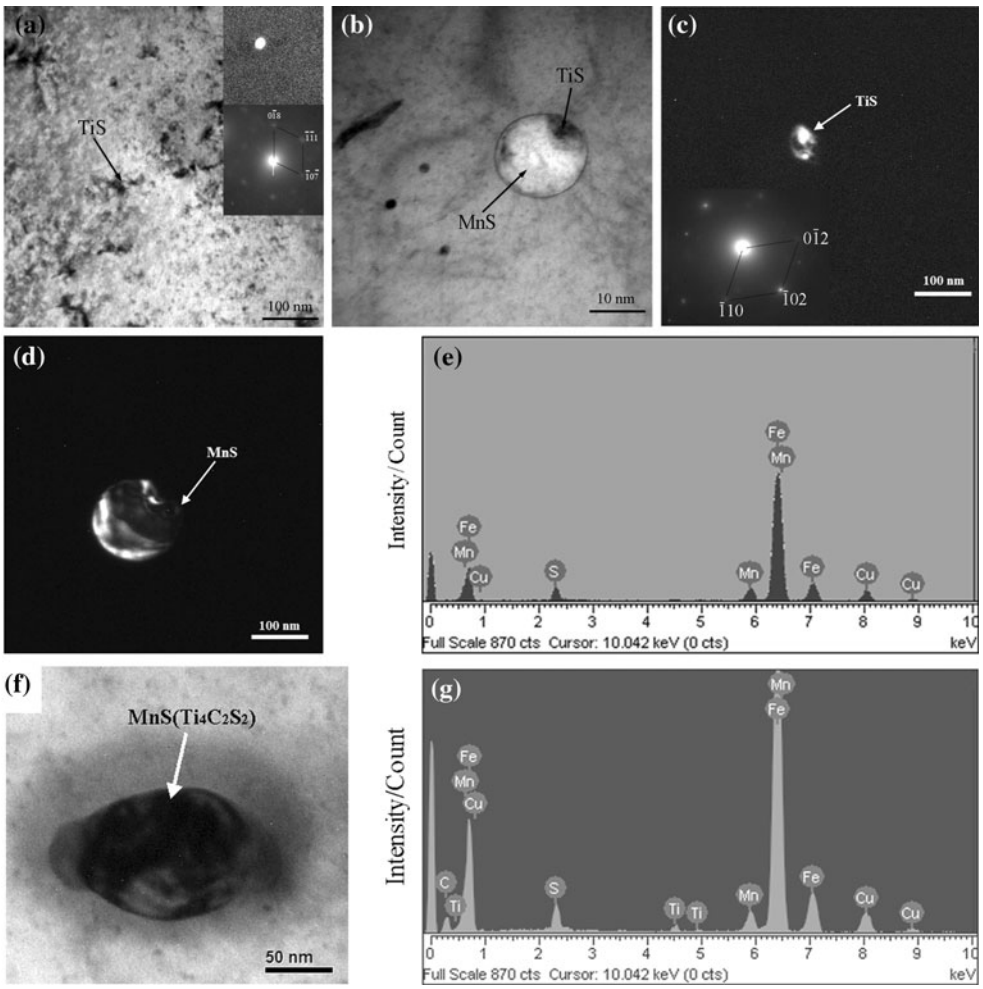

Fig. 5 Precipitates, as depicted by bright field and dark field TEM micrographs, electron diffraction pattern, EDS spectrum of **a** TiS, **b–e** compound of MnS and TiS, **f**, **g** compound of MnS and $Ti_4C_2S_2$ in Ti–V–P steel

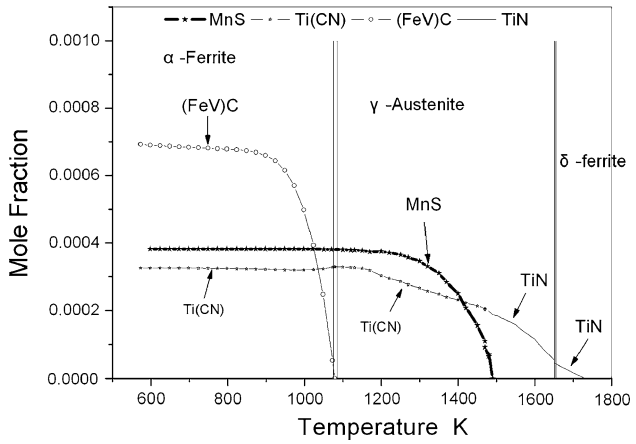

Fig. 6 Calculation results of precipitates mole fraction as function of temperature in Ti–V steel

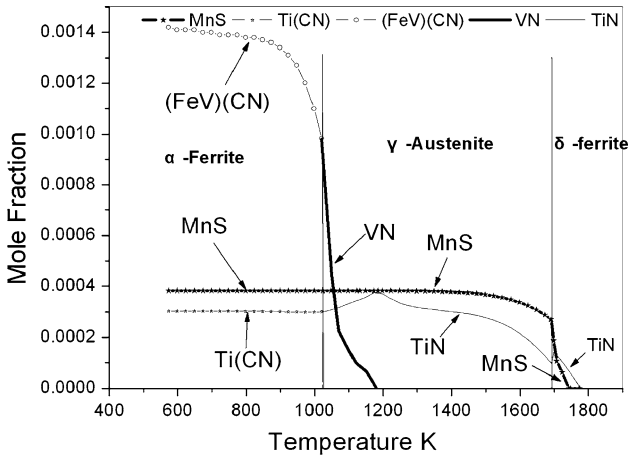

Fig. 7 Calculation results of precipitates mole fraction as function of temperature in Ti–V–Mn steel

which make it difficult to distinguish. Thus, we do the calculation in three temperature ranges within which the matrix of the steel is α-ferrite, γ-austenite, and δ-ferrite, respectively. In the α-ferrite matrix below 1079 K, two compounds of fcc structure appear. To characterize the precipitates, compositions of the two compounds are calculated, which indicate that one compound is (Fe, V)C, and the other compound is Ti(C, N). In the temperature range from 1079 K to 1654 K, only one compound of fcc structure is present except for the γ-austenite matrix.

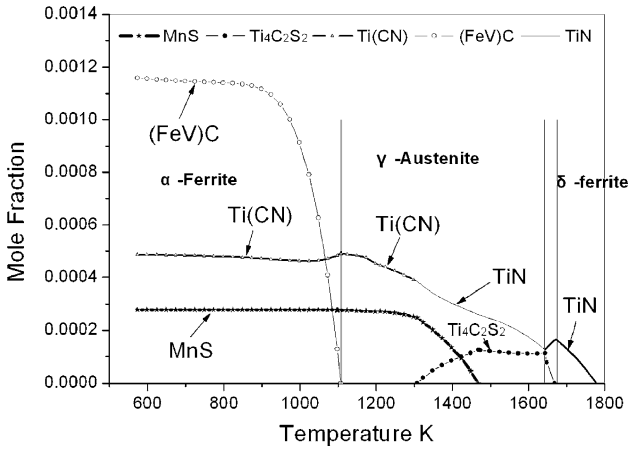

Fig. 8 Calculation results of precipitates mole fraction as function of temperature in Ti–V–P steel

Composition of this precipitate is Ti(C, N) according to the calculation results. Above 1654 K in the matrix of δ-ferrite, TiN precipitate is present. All precipitates are clearly distinguished and the mole fractions of precipitates as functions of temperature in Ti–V steel are shown in Fig. 6.

Similarly, mole fractions of precipitates in Ti–V–Mn and Ti–V–P steels are calculated and the results are shown in Figs. 7 and 8, respectively.

Results from thermodynamic calculations illustrate that three common precipitates, i.e. Ti(C, N), MnS, and (Fe, V)C are formed in the above three ULC-BH steels. However, some VN precipitate is observed in austenite field in Ti–V–Mn steel, which is probably because the residual N element tends to combine with V after being fixed by Ti (see Fig. 7). By comparison, one distinct difference in Ti–V–P steel is that some $Ti_4C_2S_2$ precipitates are present in the sample (see Fig. 8). Moreover, the calculation results also predict that TiN precipitation occurs at 1733 K (1460 °C) in Ti–V steel, while at 1773 K (1500 °C) in Ti–V–Mn and Ti–V–P steels. Obviously, the addition of Mn or P increases the initial precipitation temperature of TiN. For samples of Ti–V, Ti–V–Mn, and Ti–V–P steels, it is clearly demonstrated by the calculation results that MnS precipitation occurs at 1480 K (1207 °C), 1743 K (1470 °C), and 1473 K (1200 °C), respectively, indicating that the addition of Mn in Ti–V–Mn steel greatly promotes the precipitation of MnS.

Comparing the SEM and TEM result with the calculation result, it can be found that some of the precipitates, such as MnS, $Ti_4C_2S_2$, VC, etc. are same in the two results. However, there are some differences in the two results because the steels are calculated in the equilibrium state which is different from the real state in this investigation. For example, precipitates of titanium sulfide, manganese carbide, TiS, Ti_2N, V_2C, and V_6C_5 in the SEM and/or TEM result are not clearly present in the calculation result.

3DAP results and discussions

The distribution of solute elements in Ti–V–Mn and Ti–V–P steels are examined and shown in Figs. 9 and 10, respectively.

According to the 3DAP results, no free Ti, N, or S atoms are present in the two steels, indicating their full presence in precipitates. In Ti–V–Mn steel, the cluster of C and V with dimension of several nanometers is found in the matrix (Fig. 9a–c), and this is consistent with the TEM results (Fig. 4a, b), indicating that sizes of the particles of vanadium carbides in the matrix are mostly several nanometers. Besides, 3DAP result shows that the concentration of C is 0.00128 wt% in the matrix, a rather low but reasonable value considering that most of the carbides tend to precipitate during hot-rolling process and the following cooling cycle. However, up to 0.05 wt% (0.09 wt%

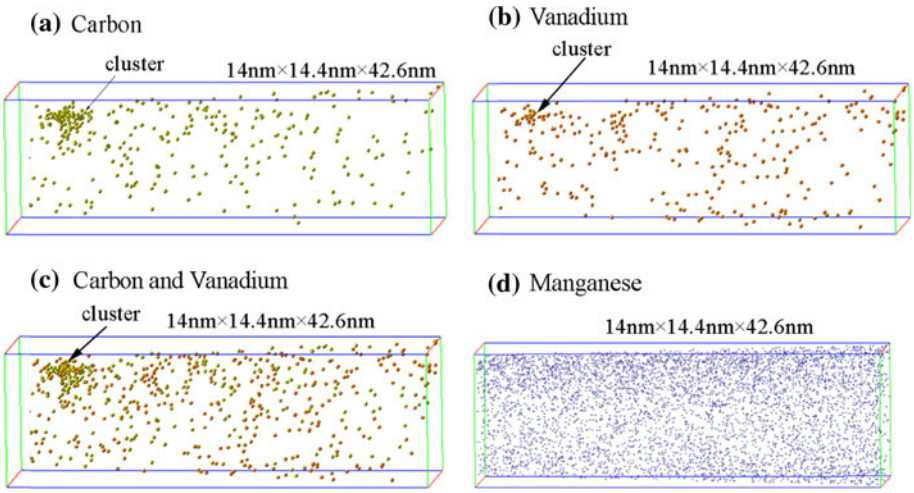

Fig. 9 Cluster of **a** C, **b** V, **c** C and V and uniform distribution of **d** Mn in Ti–V–Mn steel detected by 3DAP

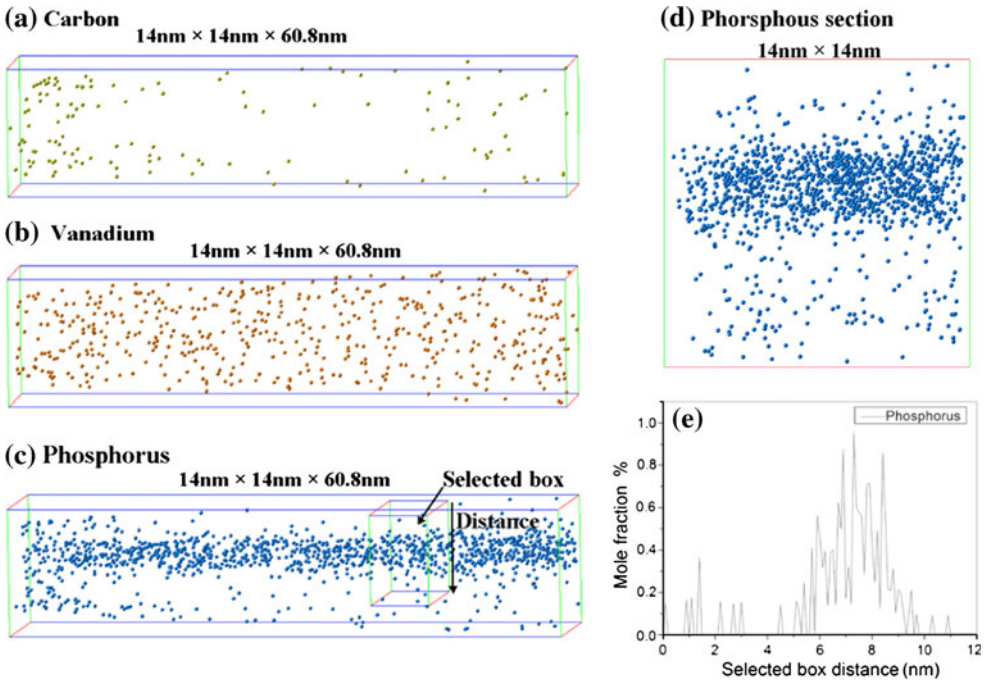

Fig. 10 Solute elements of **a** C, **b** V and **c–e** P (with **c** distributions of P along length and **d** along transverse section, **e** change of its mole fraction with distance in selected box) in Ti–V–P steel detected by 3DAP

addition) V is dissolved in Ti–V–Mn steel, which indicates that much V is left after reacting with C and N. Furthermore, as is shown in Fig. 9d, much solute Mn (mean concentration of 0.848 wt% in the observed area) distributes homogeneously in matrix.

In Ti–V–P steel, however, no clusters of C and V are found, and the mean concentration of solute V in the matrix (see Fig. 10b) is 0.054 wt%, a value similar to that in Ti–V–Mn steel. Besides, the concentration of solute C is 0.0033 wt%, which is quite low (see Fig. 10a) and also similar to that in Ti–V–Mn steel. Considering that the addition amount of C and V in the two ULC-BH steels are similar, the above results demonstrate that amount of precipitates of vanadium carbides in Ti–V–P steel is no less than that in Ti–V–Mn steel, and most of them precipitate over other particles as described in "SEM results and discussions" section, since no VC particles precipitated alone are observed in TEM result (Fig. 5). Furthermore, Fig. 10c–e shows the distribution pattern of solute P in the sample of Ti–V–P steel, from which it can be concluded that P is segregated in some place of the matrix, like grain boundary mentioned by Dionne et al. [30]. Because of its segregation, concentration of solute P in some area reaches up to 0.078 wt%, a value much higher than its bulk concentration (0.054 wt%). This result is consistent with those of SEM, TEM, and *Thermo-Calc*, and all of these evidences demonstrate the absence of the P containing precipitate. It can be concluded that P is totally dissolved in the hot-rolled ULC-BH steel, though its bulk concentration is high up to 0.054 wt%.

Conclusions

The effect of Mn and P on types of precipitates as well as solute distributions in ULC-BH steels are investigated in the present work. The following conclusions can be obtained.

The addition of Mn and P increases the initial precipitation temperature of TiN by approximately 40 °C. Meanwhile, the addition of Mn increases this temperature by about 300 °C.

The addition of Mn in BH steel induces the formation of complicated compound and decreases the solubility of C. Besides, dimensions of most vanadium carbides are tens of nanometers in Ti–V–Mn steel. In Ti–V–P steel, however, more vanadium carbides precipitate over manganese sulfide and titanium sulfide rather than exist alone. Much nanometer-sized particles of manganese sulfide precipitate in the steel, part of which precipitate together with TiS (or $Ti_4C_2S_2$). In addition, P contained particles are not found in the sample of Ti–V–P steel.

No free Ti, N, or S atoms are dissolved in the samples of Ti–V–Mn and Ti–V–P steel, whereas in both steels, little C and much V are dissolved in the matrix. In Ti–V–Mn steel, addition of Mn induces the clusters of V and C with the size of several nanometers in the matrix. Moreover, much solute Mn distributes homogeneously in the matrix. In Ti–V–P steel, however, no clusters of V and C are observed. P is totally dissolved and segregated in the matrix even though its concentration is so high up to 0.054 wt% in hot-rolled ULC-BH steels.

Acknowledgements The authors are grateful to National Basic Research Program of China (973) under Grant No. 2010CB630802 for the project funding, National Nature Science foundation of China program under Grant Nos. 50934011 and 50971137 for their financial supports. Dr. Liu Wenqing and Mr. Peng Jianchao are also acknowledged for their help in 3DAP test and TEM measurement.

References

1. Tanioku T, Hoboh Y, Okamoto A, Mizui N (1991) Development of a new bake-hardenable galvannealed sheet steel for automotive exposed panels. SAE Technical Paper 910293. Warrendale, PA, p 303
2. Ooi SW, Fourlaris G, Tanner DA, Robinson JS (2006) Mater Sci Technol 22:525
3. Ooi SW, Fourlaris G (2006) Mater Charact 56:214
4. Taylor KA, Speer JG (1997) In: 39th MWSP conference Proceedings ISS, vol XXXV. Indianapolis, IN, USA, p 49
5. Al-Shalfan W, Speer JG, Findley K, Matlock DK (2006) Metall Mater Trans A 37A:206
6. Girina O, Bhattacharya D (1999) In: 41st MWSP conference proceedings ISS, vol XXXVII. p 435
7. Al-Shalfan W, Speer JG, Matlock DK, Kim S, Ledbetter H (2000) In: 42nd MWSP conference proceedings, p 741
8. Das SK, Chatterjee S, Tarafder S (2009) J Mater Sci 44:1094. doi:10.1007/s10853-008-3106-z
9. Kamada Y, Takahashi S, Kikuchi H, Kobayashi S, Ara K, Echigoya J, Tozawa Y, Watanabe K (2009) J Mater Sci 44:949. doi:10.1007/s10853-008-3182-0
10. Miller MK (1999) Science 286:2285
11. Yamaguchi Y, Takahashi J, Kawakami K (2009) Ultramicroscopy 109:541
12. Blavette D, Déconihout B, Chambreland S, Bostel A (1998) Ultramicroscopy 70:115
13. Menand A, Cadel E, Pareige C, Blavette D (1999) Ultramicroscopy 78:63
14. Hono K (1999) Acta Mater 47:3127
15. Ping DH, Hono K, Nie JF (2003) Scripta Mater 48:1017
16. Oh JC, Ohkubo T, Mukai T, Hono K (2005) Scripta Mater 53:675
17. Wilde J, Cerezo A, Smith GDW (2000) Scripta Mater 43:39
18. Caballero FG, Miller MK, Babu SS, Garcia-Mateo C (2007) Acta Mater 55:381
19. Pereloma EV, Timokhina IB, Miller MK, Hodgson PD (2007) Acta Mater 55:2587
20. Vaumousse D, Cerezo A, Warren PJ (2003) Ultramicroscopy 95:215
21. Wen YT, Su QM, Wuttig M (1998) In: 40th MWSP conference proceedings ISS. p 833
22. Wen YT, Su QM, Wuttig M (1998) In: 39th MWSP conference proceedings ISS, vol XXXV. p 271
23. Saitoh H, Ushioda K (1993) Mater Trans JIM 34:13
24. Okamoto A, Mizui N (1990) ISIJ Jpn 76:422
25. Medina SF, Gómez M, Gómez PP (2010) J Mater Sci 45:5553. doi:10.1007/s10853-010-4616-z
26. Ghosh P, Ghosh C, Ray RK, Bhattacharjee D (2008) Scripta Mater 59:276
27. Thermo-Calc AB. TCFE6, Thermo-Calc Software AB Steel Database, Version 6. Stockholm: Thermo-Calc AB; (2006)
28. Calliari I, Brunelli K, Zanellato M, Ramous E, Bertelli R (2009) J Mater Sci 44:3764. doi:10.1007/s10853-009-3505-9
29. Vasconcelos I, Tavares S, Reis F, Abreu H (2009) J Mater Sci 44:293. doi:10.1007/s10853-008-3064-5
30. Dionne S, Essadiqi E, McMahon G, Martin P et al (1999) In: 41ST MWSP conference proceedings ISS, vol XXXVII. p 235